Phase Behavior of Poly(propylene oxide)-Poly(ethylene oxide)-Poly(propylene oxide) Triblock Copolymer Melt and Aqueous Solutions

Kell Mortensen*

Department of Solid State Physics, Risø National Laboratory, DK-4000 Roskilde, Denmark

Wyn Brown

Department of Physical Chemistry, University of Uppsala, S-75121 Uppsala, Sweden

Erling Jørgensen

Roskilde University Center, DK-4000 Roskilde, Denmark

Received June 1, 1994®

ABSTRACT: Structural studies are presented on the Pluronic-R copolymer 25R8, which has a central poly(ethylene oxide) block (80 wt % of the copolymer) symmetrically surrounded by poly(propylene oxide) blocks. The studies include small-angle neutron scattering, static and dynamic light scattering, and rheology. Complex aggregation behavior is observed as a function of temperature and copolymer concentration. At low temperatures and low copolymer concentrations the $(PO)_n(EO)_m(PO)_n$ copolymers are dissolved as independent macromolecules. In a wide temperature range of dilute concentrations, the scattering patterns indicate formation of large domains of networks of copolymer strands interconnected randomly through the hydrophobic poly(propylene oxide) end blocks. At higher copolymer concentrations an interconnected network of micelles is formed in which micellar cores of hydrophobic poly(propylene oxide) are interconnected by poly(ethylene oxide) strands. For concentrations above 50 wt % this network constitutes the whole sample, resulting in a transparent homogeneous phase. Close to 60% copolymer concentration, the micellar network forms a low-temperature ordered solid-like mesophase. At higher polymer concentrations and low temperatures an elastic two-phase system is formed of a coexisting swollen lamellar and micellar network. In the pure melt, the 25R8 triblock copolymer forms a lamellar structure below T_m = 55 °C.

I. Introduction

Polymeric surfactants have recently attracted great interest, both as a result of their commercial utility and because of their novel physical behavior. Especially, many studies have been performed on aqueous solutions of the block copolymer PEO-PPO-PEO, where PEO is poly(ethylene oxide) and PPO is poly(propylene oxide).[1-10] It is now well established that these block copolymers associate into micellar aggregates of spherical, rodlike, or possibly layered forms, depending on molecular design and temperature.[7,8,11] These micellar aggregates constitute the basis for a variety of crystalline mesophases.[3,4] In some respects, these block copolymer surfactants thus behave as typical low-molecular-weight amphiphiles. There are important differences, though: the triblock copolymer systems have, for example, no clear distinction between lyotropic and thermotropic phase behavior.

The proven commercial utility of the PEO-PPO-PEO surfactant macromolecules has led to further research to find structural modifications that would offer even broader selections of surfactant properties and characteristics. Reversal of the hydrophobic and hydrophilic blocks in the PPO-PEO-PPO triblock copolymer (Pluronic-R) is among such new candidates.[12] In aqueous solutions, these PPO-PEO-PPO copolymers show distinct differences from the related PEO-PPO-PEO copolymers. Of particular interest are the low foaming and good wetting properties. Among the utilities are cleaning agents in such products as cosmetic face creams, shampoos, and lotions and dispersants for printing inks, paints, and coatings.

The present paper describes the elucidation of the structural properties of D_2O solutions of a copolymer having a long central chain of PEO and relatively short chains of PPO made over the entire span of concentrations from dilute up to the melt and over a broad range of temperatures. Rheological measurements on the suspensions are also made.

II. Experimental Section

A. Material. The triblock copolymer poly(propylene oxide)-poly(ethylene oxide)-poly(propylene oxide), $[OCH_2CH(CH_3)]_m$-$H[OCH_2CH_2]_n[OCH_2CH(CH_3)]_m$ or $(PO)_m(EO)_m(PO)_m$ (or PPO-PEO-PPO), abbreviated 25R8, was obtained from BASF Corp., Wyandotte, MI. The molecular weight of the copolymer given by the manufacturer[12] is M_{25R8} = 8550, corresponding to M_{PEO} = 6840 and M_{PPO} = 1710. Since the molar mass of ethylene oxide equals 44 and that of propylene oxide equals 58, this gives the corresponding polymerization degrees m = 15 and n = 156.

The triblock copolymer was used without further purification. For concentrations below 50 wt %, the copolymer was dissolved in D_2O at 5 °C, in which it forms a homogeneous solution. The high-concentration solutions were prepared at ambient temperature and then heated to roughly 60 °C to make a homogeneous sample. The samples were sealed and stored at high temperature for more than 24 h to reach equilibrium. Deuterium oxide (D_2O) was used to get good contrast and low background in the neutron scattering experiments. The solutions discussed below are all given in weight percent (wt %).

B. Small-Angle Neutron Scattering. Small-angle neutron scattering experiments were performed using the Risø SANS facility, which is a flexible instrument covering scattering vectors from 0.002 to 0.5 Å^{-1} with variable neutron wavelength resolution.

The samples were mounted in sealed quartz containers (Suprasil from Hellma, FRG) with a 2 mm flight path. The 80 wt % sample was in addition studied when mounted in a sealed Couette type of shear cell.[13] The shear cell was used to study possible structural dependence on shear.

Most of the results presented below were obtained using neutrons with 6 Å wavelength with sample-to-detector distances of 3 m, giving scattering vectors in the range 0.01-0.1 Å^{-1}, where

® Abstract published in *Advance ACS Abstracts*, August 15, 1994.

0024-9297/94/2227-5654$04.50/0

the scattering vector $\bar{q}$ is given by the scattering angle θ and the neutron wavelength λ:

$$|\bar{q}| = q = (4\pi/\lambda)\sin(\theta/2)$$

A few representative experiments were measured with an extended q-range, using neutron wavelengths of 3 and 10 Å and 1 and 6 m sample-to-detector distances, respectively. The neutron wavelength resolution was $\Delta\lambda/\lambda = 0.18$, the neutron beam collimation was determined by pinhole sizes of 16 and 7 mm diameter at the source and sample positions, respectively, and the collimation length was equal to the sample-to-detector distance. The smearing induced by the wavelength spread, the collimation, and the detector resolution was included in the data analysis discussed below, using Gaussian approximations for the different terms.[14]

The scattering data were corrected for the background arising from either the quartz cell or the Couette cell with D_2O and from other sources, as measured with the neutron beam blocked by plastic containing boron at the sample position. The incoherent scattering from H_2O was used to determine deviations from a uniform detector response and to convert the data into absolute units.

The scattering patterns discussed in the present paper are all, except for the 65 wt % sample at low temperature and the 80 wt % sample when exposed to shear, azimuthally isotropic. The data have by azimuthally averaging been reduced to the one-dimensional $I(q)$ scattering functions, which are only dependent on the absolute value of $\bar{q}$. Temperature-dependent neutron scattering data were obtained in both heating and cooling cycles to check reproducibility. Only in the high-concentration part of the phase diagram, where a two-phase system is observed, did we observe some history and time dependence in the scattering function. Qualitatively, the data are reproducible also in the two-phase regime, but the relative importance of the two coexisting phases depends on time and history.

C. Light Scattering. Dynamic light scattering measurements were made using the technique and apparatus described earlier[15] equipped with an Ar ion laser (Coherent Radiation Model Innova 300) emitting vertically polarized light (Glan-Thompson polarizer, extinction better than 10^{-6}) with wavelength 488 nm and an ALV-5000 multibit, multi-τ full digital autocorrelator. The detector optics employed a 4 μm diameter monomodal fiber coupled to the photomultiplier. Measurements of depolarized dynamic light scattering were also made on the 25R8 melt. The scattered light at angle 90° passed through a Glan-Thompson polarizer with an extinction coefficient better than 10^{-7}, whose orientation was adjusted to give the minimum intensity for a dilute solution of a high-molecular-weight polystyrene in ethyl acetate. Intensity light scattering measurements were made using a photon-counting device supplied by Hamamatsu. The light source was a 3 mW He–Ne laser (λ = 633 nm). The optical constant for vertically polarized light is

$$K = 4\pi n_0(dn/dc)^2/N_A\lambda^4$$

where n_0 is the solvent refractive index, dn/dc is the refractive index increment, which was measured using a specially constructed differential refractometer with Rayleigh interference optics ($(dn/dc) = 0.131$ mL/g at 633 nm), and N_A is Avogadro's number. R_θ is the Rayleigh ratio obtained by calibration measurements with benzene: $R_{90°} = 11.85 \times 10^{-6}$ cm^{-1} at 25 °C.

D. Rheology. Viscoelastic measurements were performed on a Bohlin VOR rheometer with a fluid bath temperature control. A stainless steel Couette measuring cell, C14 (inner diameter 14.0 mm, outer diameter 15.4 mm, and height 21 mm), was used for all measurements. Storage and loss moduli, G' and G'', were measured as a function of temperature. The frequency of oscillation was 0.15 Hz and the strain amplitude was less than 0.004. The heating and cooling rates were ±0.25 °C/min. The frequency dependence was measured at a strain amplitude of 0.004, and the strain dependence at a frequency of 0.15 Hz.

The oscillatory measurements were made on solutions with concentrations between 20 and 75 wt %. The samples were placed in the Couette cell, as a liquid, at high temperature.

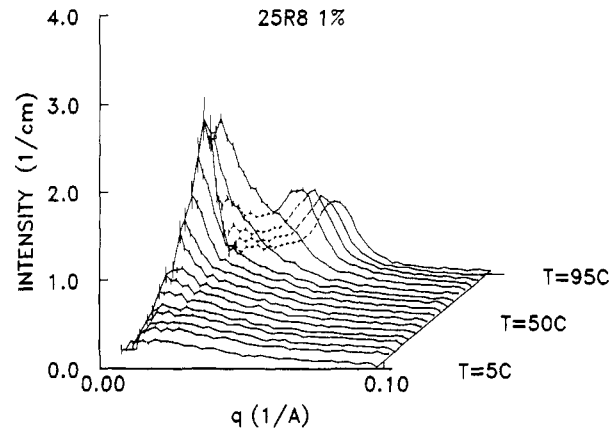

Figure 1. Neutron scattering data of 1 wt % 25R8 as measured in the temperature range 5–95 °C.

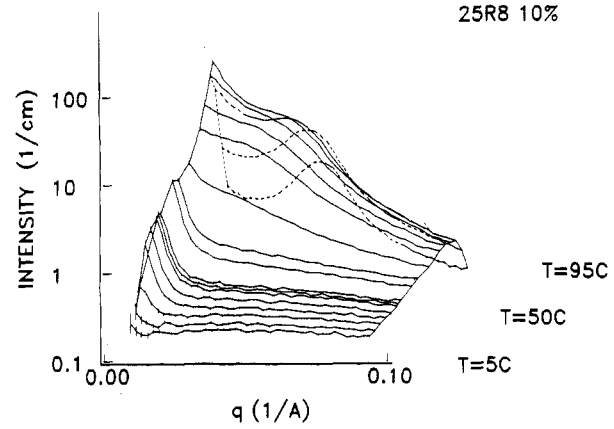

Figure 2. Neutron scattering data of 10 wt % 25R8 as measured in the temperature range 7–85 °C.

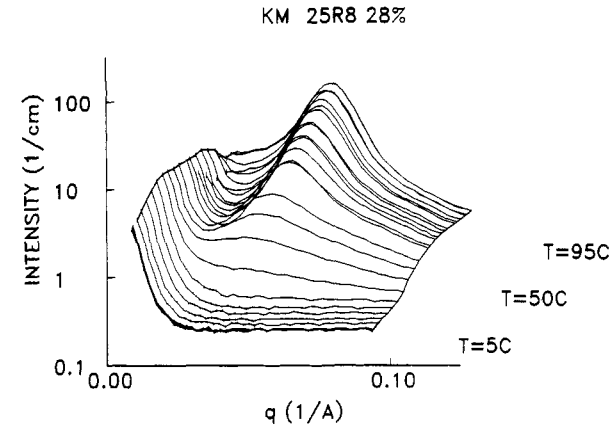

Figure 3. Neutron scattering data of 28 wt % 25R8 as measured in the temperature range 8–88 °C.

III. Results and Discussion

Figures 1–6 show characteristic neutron scattering data for 25R8 dissolved in D_2O at polymer concentrations of 1, 10, 28, 50, 65, and 80 wt %, respectively. The low-concentration samples all show rather similar behavior, with weak scattering at low temperatures, markedly increased small-angle scattering at intermediate temperatures, and a pronounced correlation peak at the highest temperatures. This correlation peak appears at a lower temperature the higher the copolymer concentration. For intermediate concentrations, represented by the c = 50 and c = 65 wt % suspensions, the scattering pattern is dominated by the correlation peak over the whole temperature range measured. At low temperatures, a solid homogeneous gel is formed for concentrations between

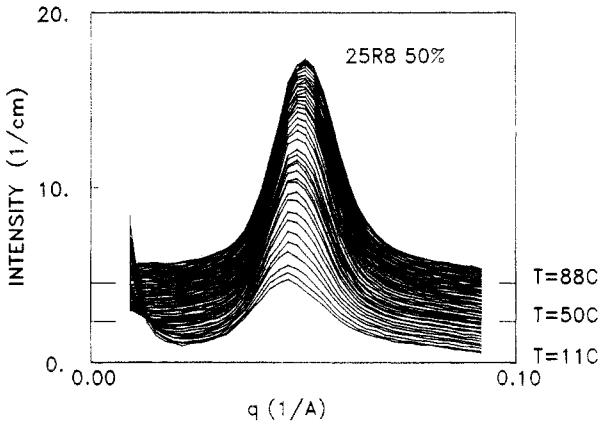

Figure 4. Neutron scattering data of 50 wt % 25R8 as measured in the temperature range 10–85 °C. The scattering curves are displaced proportional to the temperature, as indicated on the right axis.

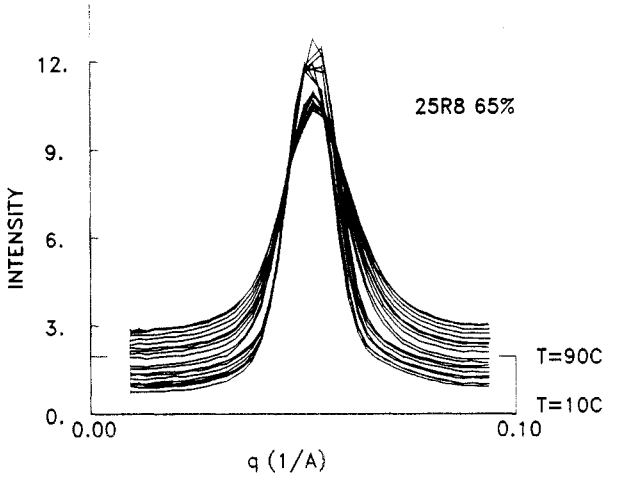

Figure 5. Neutron scattering data of 65 wt % 25R8 as measured in the temperature range 10–91 °C. The scattering curves are displaced proportional to the temperature, as indicated on the right axis.

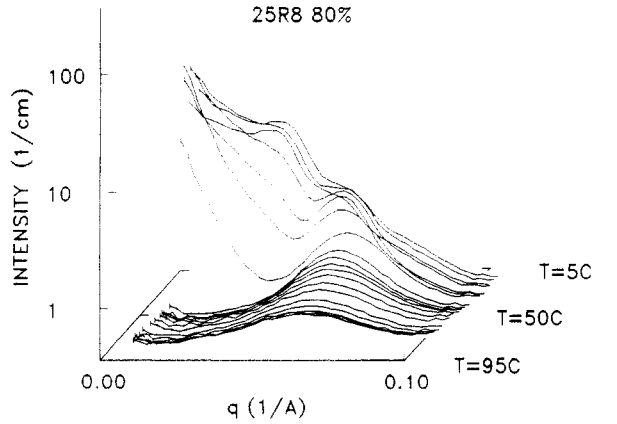

Figure 6. Neutron scattering data of 80 wt % 25R8 as measured in the temperature range 10–86 °C.

approximately 50 and 65 wt %. For even higher copolymer concentrations, a pronounced correlation peak is restricted to only a narrow temperature range. However, a weak peak in $S(q)$ is observed up to the highest temperatures. At lower temperatures and at high concentrations, a gel is formed with anisotropic scattering characteristics.

As the concentration is increased above 10 wt %, solutions of 25R8 become turbid at ambient temperature. At c = 45 wt % the solutions form a milky liquid below 55 °C. This precludes light scattering measurements in large parts of the phase diagram. At higher temperatures with the concentrated solutions, however, a stable, viscous glass-clear phase is formed. At even higher concentrations, 25R8 forms either a highly viscous glass-clear solution or a glass-like gel below a minimum temperature depending on the particular concentration. A solution of 80 wt % is not optically clear but has a "grainy" two-phase texture. With temperature reduction, the demixing process at a given concentration is not sharp, however, and proceeds slowly over several hours.

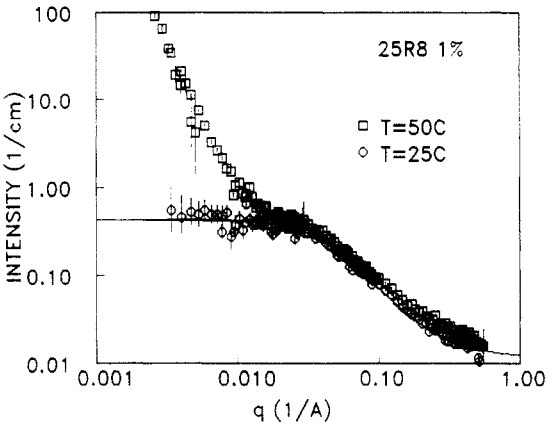

Figure 7. Neutron scattering data of 1 wt % 25R8 as measured at T = 25 °C (○) and T = 50 °C (□). The shown scattering functions are combined data of (λ; sample-to-detector distance) = (3 Å; 1 m), (6 Å; 3 m), and (10 Å; 6 m) settings, λ being the neutron wavelength. The solid line represents the fit to the Debye function, giving R_g = 37 Å.

Total intensity light scattering measurements were made on 25R8 in dilute solution in D_2O over the range 0.5–10 wt %.

Dynamic light scattering (DLS) measurements were made on the same solutions. In addition, DLS was made on selected concentrated solutions with concentrations of 45, 54, 64, 73, and 91 wt % at temperatures between 40 and 80 °C and on 64 wt % down to 6 °C.

In the following, we will present and discuss the experimental observations in each of the identified phases.

A. Unimers. At low temperatures, the dilute copolymer suspensions form a transparent liquid of low viscosity. Both the neutron and the light scattering data indicate scattering from relatively small objects.

A1. Neutron Scattering. In the dilute solutions, the small-angle neutron scattering experiments show weak scattering at low temperature with a q-dependence which resembles the Debye function

$$I(q) = [cMN_A(\Delta b)^2][1/x^{-2}(e^{-x} + x - 1)] + I_{inc} \quad (1)$$

thus indicating that the copolymers are dissolved as individual chains with a random coil conformation. In the Debye function, $x = (qR_g)^2$, R_g being the radius of gyration. $\Delta b = \sum b - \rho_s V_{25R8}/M_{25R8}$ is the contrast factor, where $\sum b$ is the total coherent scattering length of one molecule, $M = M_{25R8}$ and V_{25R8} are respectively the molecular mass and dry volume of a 25R8 copolymer, and ρ_s is the scattering length density of D_2O. For 25R8 in D_2O, $\Delta b = 9.8 \times 10^{-14}$ cm. N_A is Avogadro's number, c is the copolymer concentration, and I_{inc} is the incoherent scattering from the sample.

Fits of the Debye function to the experimental 1 wt % data are shown in Figure 7 and result in a zero-q value, $I(q=0)$ = 0.46 cm^{-1}, corresponding to $M_{25R8} = 8 \times 10^3$, in good agreement with the molecular weight of M_{25R8} = 8550 given by BASF[12] and the light scattering data presented

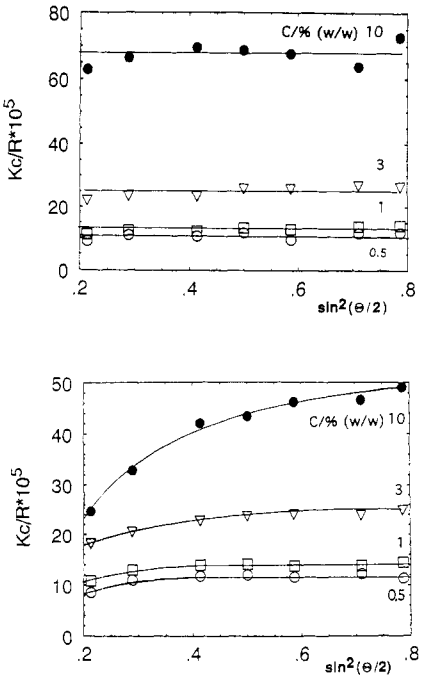

Figure 8. Angle dependence of the intensity light scattering data for dilute solutions of 25R8 in D_2O at the concentrations shown: (a) T = 10 °C; (b) T = 15 °C.

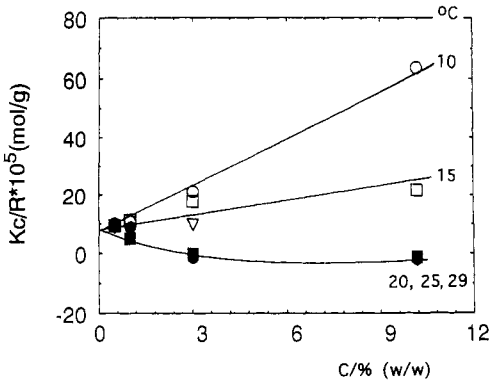

Figure 9. Concentration dependence of intensity light scattering data for 25R8 solutions in D_2O at the different temperatures shown.

below. The radius of gyration obtained from a fit to eq 1 is R_g = 37 Å.

The 10 wt % solution also shows weak scattering at the lowest temperatures measured. Already at 5 °C, however, additional small-angle scattering reveals some aggregation, although the dominant behavior is still that of the single chain.

A2. Light Scattering. While the dilute solutions were optically clear at lower temperatures, the scattering intensity provides strong evidence for aggregation with increasing temperature and concentration. Figure 8a shows the reduced scattered intensity (Kc/R_θ) as a function of $\sin^2(\theta/2)$ at 10 °C: there is no significant angular dependence for the concentrations used. For 15 °C, however, there is a low-angle dependence of the reduced intensity which increases with increasing concentration (Figure 8b).

The concentration dependence of (Kc/R_θ) extrapolated to θ = 0 is shown in Figure 9. The intercept at c = 0 corresponds approximately to the theoretical molecular weight for the copolymer (given by the manufacturers) of 8550.

Dynamic light scattering measurements were performed on the same solutions. The correlation functions in Figure

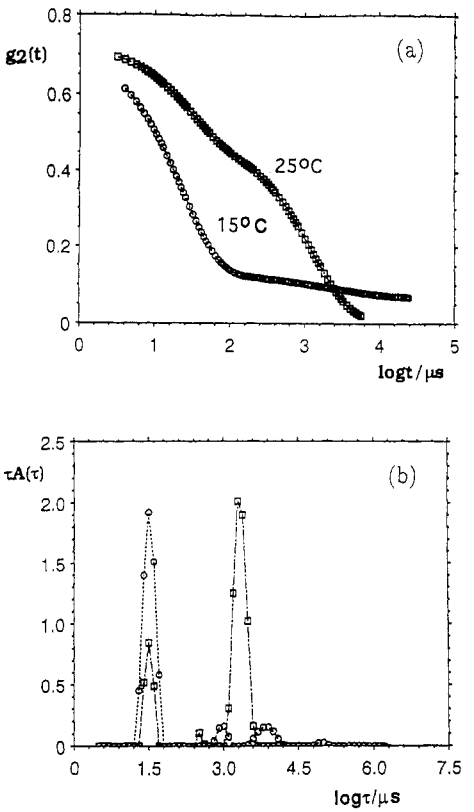

Figure 10. Dynamic light scattering data for a 3% 25R8 solution in D_2O. (a) Intensity–intensity correlation function ($g_2(t)$) at 15 °C at 25 °C at angle 90°. (b) Inverse Laplace transform (ILT) of the data in (a) ((○) 15 °C; (□) 25 °C).

10a for the 3 wt % solution show that at 15 °C the data are close to a single exponential with a low-amplitude slow component. At 25 °C the slow mode is dominant. Figure 10b shows the corresponding inverse Laplace transform (ILT) for the data. From the relaxation rate of the fast component, the hydrodynamic radius corresponding to the unimer at c = 3 wt % is found to be R_h = 23 Å.

B. Random Network. Over a relatively wide temperature range for both the dilute and the relatively concentrated suspensions (c < 40 wt %), the samples are characterized by an intense neutron scattering at zero momentum transfer. In light, this can be seen directly as the material is turbid. The neutron scattering data provide a q^{-4} dependence at low q. These observations indicate the formation of macroscopic-sized clusters and constitute within this regime a low-viscosity suspension.

B1. Neutron Scattering. As mentioned above, the 10 wt % solution shows at 5 °C additional small-angle scattering, revealing some aggregation. At approximately T = 20 °C there is a marked increase in $I(q)$, which reveals major molecular association. The scattering function of the 1 wt % dispersion shows a corresponding low-q dominance for temperatures above approximately 45 °C, whereas the 28 wt % dispersion shows such behavior already at the lowest temperature measured (5 °C). Within the same range of temperature and concentrations the dispersions become turbid.[12]

The character of the scattering pattern, i.e., intense $I(q$=0) behavior, is observed for temperatures up to approximately T = 80 °C for both 1 wt % (Figure 1) and 10 wt % suspensions (Figure 2), whereas the 28 wt % sample (Figure 3) shows such behavior up to approximately T = 40 °C. Above these temperature limits, a correlation peak appears, as discussed below. There is, however, not a sharp transition between the high- and the low-temperature limits. A significant $I(q$=0) tail coexists at

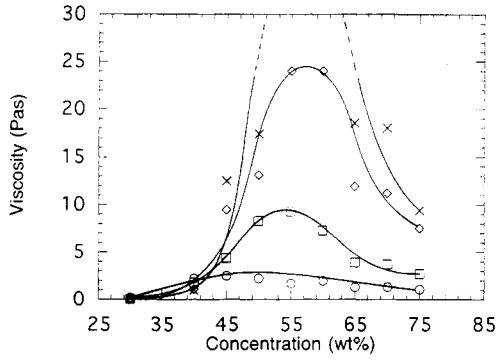

Figure 11. Viscosity of 25R8 suspensions measured at the temperatures 40 (×), 45 (◇), 60 (□), and 80 °C (○) as a function of copolymer concentrations. At T = 40 °C, the 55 and 60 wt % suspensions form solid phases.

high temperatures, with the correlation peak extending over a 10–20 °C temperature range.

While the low-q scattering is the dominant property within this temperature range, only minor changes appear at high q values, as seen in Figure 7. The scattering function thus indicates that large clusters or a very inhomogeneous random network is formed, in which most of the PPO–PEO–PPO chain, presumably the central PEO block, keeps the original conformation, whereas the hydrophobic PPO blocks associate and act as knots in a network (see also Figure 30).

B2. Light Scattering. At approximately 15 °C a strong angular dependence appears in the low-angle range of the scattered light (Kc/R_θ), as shown in Figure 8b. This trend increases with concentration.

At temperatures of 20 °C and above, the apparent molecular weight increases, confirming the increasing association of the copolymer 25R8 with temperature and concentration. Dynamic light scattering measurements on the same solutions substantiate these conclusions. The correlation functions in Figure 10a for the 3 wt % solution show that while at 15 °C the data are close to a single exponential at 25 °C, the function is clearly bimodal with a strong increase in the relative amplitude of the slower mode, as obtained by inverse Laplace transformation. The ILT data are shown in Figure 10b.

C. Micellar Network. At temperatures below $T \sim$ 40 °C the solution properties are those of a viscous liquid.

C1. Rheology. The viscosity η of the almost Newtonian suspension increases markedly with reduction in temperature, and at 40 °C η passes through a broad maximum as a function of concentration, centered at $c \sim$ 55 wt % (Figure 11). At 40 °C, the 55 and 60 wt % suspensions are gels.

The 45, 55, 60, and 75 wt % samples were measured in the temperature range 6–60 °C. While the 45 wt % suspension typically shows a small elastic modulus over the whole temperature range, the 60 and 75 wt % materials exhibit marked increases in G' below approximately 40 °C. Some sample dependence is seen for suspensions with concentrations below approximately 50 wt %. While these suspensions sometimes, at low temperatures, appear as opaque low-viscosity materials, they have also been observed as transparent samples with moderate modulus. Figure 22 gives more detailed moduli data on 25R8 suspensions. At high temperatures all samples show only small elastic moduli.

C2. Neutron Scattering. At temperatures above approximately 80 °C for 1 and 10 wt % and above 40 °C for the 28 wt % solution, the scattering function changes in character. The low-q scattering decreases, although it is still present, and a pronounced correlation peak appears. Such behavior is expected for a suspension of small aggregates interacting with an attractive force. It is therefore suggested that the hydrophobic PPO blocks in this temperature and concentration range assemble into relatively well-defined units, micelles, which are interconnected by the hydrophilic PEO chains, thus making a micellar network (see also Figure 30). Similar micellar networks have been observed in PS–PB–PS triblock copolymers in extender oil, where PS is polystyrene and PB is hydrogenated polybutadiene,[16] and in end-capped poly(ethylene oxide) urethanes.[17,18]

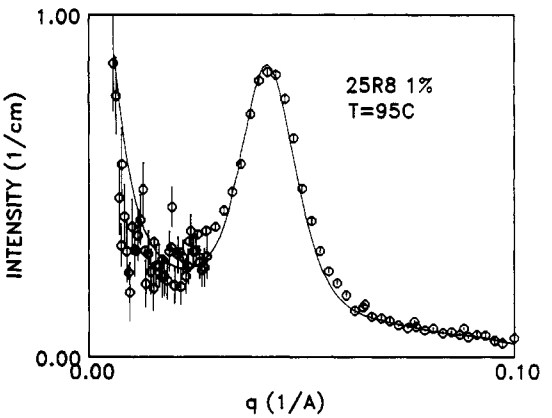

Figure 12. Neutron scattering data of 1 wt % 25R8 as measured at T = 95 °C (○). The shown scattering functions are combined data of (λ; sample-to-detector distance) = (6 Å; 3 m) and (10 Å; 6 m) settings, λ being the neutron wavelength. The solid line represents the fit to the sticky-hard-sphere model.

The scattering function can be analyzed in terms of Baxter's model for sticky hard spheres.[19] Assuming a monodisperse suspension of micelles, the scattering function can be written as the product of the single-particle form factor $P(q)$ and a structure factor, $S(q)$, describing the interparticle interference:

$$I(q) = NV^2\Delta\rho^2[P(q)\,S(q)] \qquad (2)$$

where $\Delta\rho^2$ is the contrast factor and N is the number density of scatterers. For the form factor we can apply that for a monodisperse suspension of spheres with a sharp interface,

$$P(q) = \left[\frac{3}{(qR_c)^3}(\sin(qR_c) - qR_c\cos(qR_c))\right]^2 \qquad (3)$$

characterized by the sphere radius R_c. Deviations at the largest q-values are attributed to the ethylene oxide subchains dispersed in the water phase, in agreement with a simple model of a micellar structure having a central, dense core of dominantly poly(propylene oxide) and an outer corona of hydrated poly(ethylene oxide) effectively grafted onto the surface of the core. The structure factor is given by[20]

$$S(q) = 1 + 4\pi N\int (g(R) - 1)\frac{\sin(qR)}{qR}R^2\,dR \qquad (4)$$

where $g(R)$ is the radial distribution function describing the arrangement of the micelles. Baxter showed[19] that the structure factor can be solved analytically in the Percus–Yevick approximation,[21] if the potential consists of a hard core with a rectangular attractive well.[19,22]

Figure 12 shows an example of a fit giving the Baxter stickiness parameter $b \sim$ 0.001, a hard-sphere volume fraction ϕ = 0.4, and a hard-sphere interaction radius and

core radius of respectively R_{hs} = 90 Å and R_c = 50 Å. Although the sticky hard-sphere model gives a reasonable description of the observed scattering function, we emphasize that the system is not at all uniform, and parts of the small-angle scattering may as well reflect scattering from the structure of more concentrated domains in the copolymer. The value of b should therefore be taken with some caution and will not be discussed further. The relatively high volume fraction ϕ = 0.4 can be achieved only as a result of clustering via the PEO chains, resulting in an opaque suspension in excess water. Only for copolymer concentrations above roughly 50 wt %, does the micellar network constitute the whole sample, resulting in a homogeneous transparent material.

The correlation peak, which dominates the high-temperature characteristics of the scattering function for dilute solutions, is the dominant feature over the whole temperature range for the 50 and 65 wt % suspensions, as shown in Figures 4 and 5. The peak intensity increases with increasing temperature. Simultaneously, the small-angle tail, which presumably reflects remnants of a low-temperature "random network", as discussed above, is reduced.

The 80 wt % suspension exhibits quite different characteristics (Figure 6). Within the temperature range from $T \simeq 20$ °C to T of the order of 50 °C, this material is also characterized by a correlation peak centered close to q = 0.5 Å^{-1}. At higher temperatures the peak is significantly reduced and shifts to somewhat higher q-values. Although the 80 wt % material thus shows quite different behavior from the lower concentrations, there is no indication of a phase transition to a new high-temperature phase. The change in $S(q)$ may reflect changes in the micellar characteristics. At low temperatures the intermicellar correlation peak is observed together with new features, revealing a low-temperature two-phase system, as will be discussed below.

Within most of the concentration regime associated with the micellar network, we observe only minor small-angle contributions to the scattering function. We have accordingly analyzed the data in terms of simple hard-sphere interacting micelles, using the Percus–Yevick approximation with a hard-sphere interaction potential[7,21]

$$S(q) = \frac{1}{1 + 24\phi G(2qR_{hs},\phi)/(2qR_{hs})} \quad (5)$$

where G is a trigonometric function of the hard-sphere interaction radius R_{hs} and volume fraction ϕ. We find very good fits to the data, as shown by representative curves in Figure 13. The resulting hard-sphere interaction distance varies only little with temperature and copolymer concentration. Over the whole range R_{hs} is of the order of 62–68 Å, except for the 80 wt % sample, which results in a somewhat reduced value at the highest temperatures (R_{hs} = 55 Å at 90 °C).

The resulting core radius versus temperature and polymer concentration is shown in a contour plot in Figure 14. For the 50 wt % suspension, R_c increases from R_c = 35 Å at T = 20 °C to R_c = 40 Å at T = 60 °C, with most of the T dependence below T = 40 °C. The 65 wt % material has a core size of 35–36 Å over the whole temperature range. The 80 wt % sample exhibits a significant temperature-dependent scattering function. Assuming micellar aggregates also for this high concentration, this gives R_c values which changes from R_c = 40 Å near the low-temperature phase boundary to 20 Å at 80 °C.

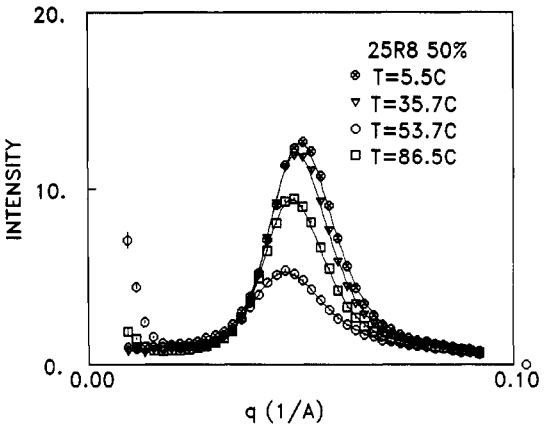

Figure 13. Representative neutron scattering data of 50 wt % 25R8 as measured at temperatures from 5.5 to 86.5 °C. The solid lines represent the least-squares fit using the Percus–Yevick hard-sphere model.

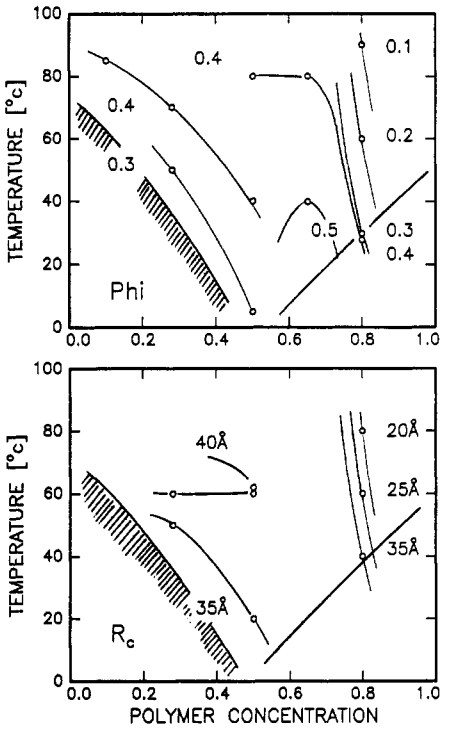

Figure 14. Contour plot of resulting hard-sphere micellar volume fraction ϕ (top) and micellar core size R_c (bottom) of 25R8 as a function of temperature and polymer concentration. The results are obtained by least squares fits of the Percus–Yevick hard-sphere approximation to the neutron scattering data.

It appears from Figure 14 that, within most of the micellar phase, the core is of the order of 35–40 Å. Assuming that the micellar core is formed by the hydrophobic poly(propylene oxide), the resulting values of R_c mean that the $(PO)_{15}$ blocks are relatively stretched going from the surface to the center region.

The effective volume fraction, as obtained from fits to the Percus–Yevick hard-sphere model, is shown as a contour plot in the top part of Figure 14. Except for the 80 wt % sample, the volume fraction changes only weakly within the 0.30–0.52 range. The low-concentration suspensions are characterized by an increasing micellar volume fraction as the temperature is increased. This is similar to the PEO–PPO–PEO systems[4,7] and may as in those systems be related to the thermodynamic equilibrium between dissolved unimers and micellar aggregates as the hydrophobic character (of PPO) changes with temperature. At higher concentrations, the temperature dependence of

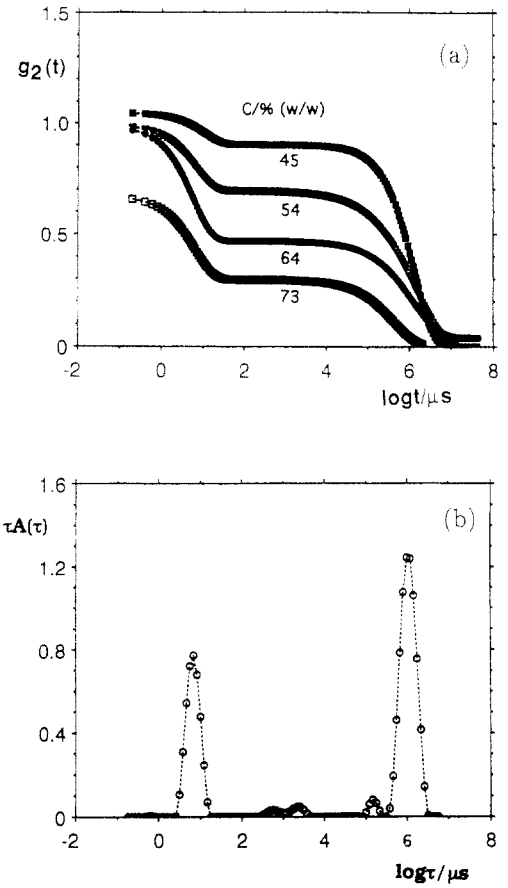

Figure 15. (a) Dynamic light scattering correlograms ($g_2(t)$) for different concentrations of 25R8 in D_2O in the range 45–73 wt % (corresponding to the micellar network in Figure 29) measured at T = 80 °C and angle 90°. (b) Inverse Laplace transform (ILT) for the correlogram at c = 73 wt %.

the micellar volume fraction is basically reversed. Upon lowering the temperature, ϕ increases. For the 50 wt % sample, ϕ increases markedly at low temperatures and reaches a weak maximum of ϕ = 0.43 around T = 50 °C, which is close to the temperature of maximum viscosity (Figure 11). The 65 wt % suspension has a constant volume fraction ϕ = 0.53 up to 40 °C, beyond which temperature it drops by about 10% within a few degrees and then further decreases slowly upon heating to ϕ = 0.4 at T = 80 °C.

C3. Light Scattering. Figure 15a shows typical polarized intensity–intensity correlation functions ($g_2(t)$) for 25R8 at concentrations between 45 and 73 wt % at 80 °C. The correlation functions are bimodal: there is a fast decay followed by a broader relaxation with a much longer delay time. Analysis was initially made using the Kohlrausch–Williams–Watts (KWW) equation:

$$g_2(t) = (A \exp(-(t/\tau)^{\beta}) + B)^2 \quad (6)$$

where β ($0 < \beta < 1$) is a fitting parameter describing the shape of the distribution and τ is an average relaxation time. Since a single KWW function is clearly unsuitable for the functions shown in Figure 15a, the correlation functions were fitted to a double KWW function. This procedure showed that the faster decay is approximately single exponential while the slower decay has a broader distribution. Subsequently, fits were made fixing the shape parameter β for the fast process to unity (i.e., a single exponential) and allowing the other parameters to float. This was found to be a satisfactory analysis method, and the curves in Figure 15a were fitted in this manner.

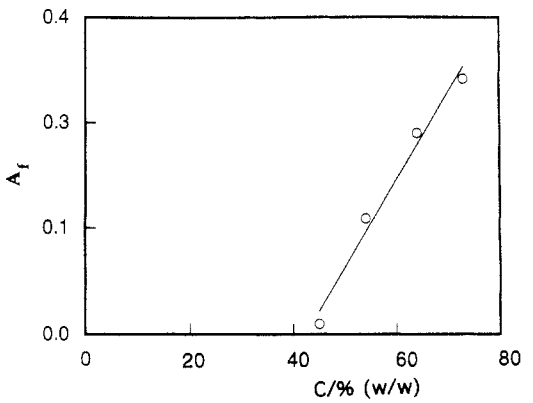

Figure 16. Relative amplitude of the fast mode from ILT of dynamic light scattering correlograms as a function of concentration for 25R8 in D_2O at 60 °C.

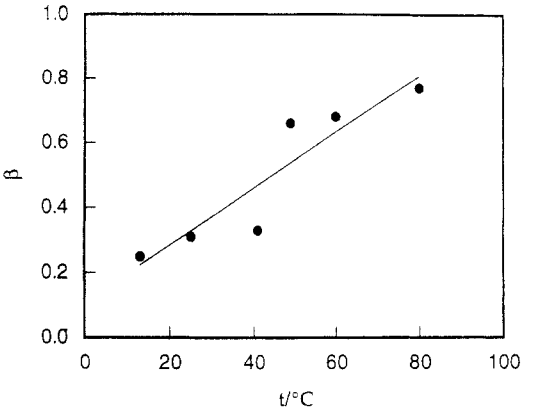

Figure 17. Shape parameter β (KWW fit, eq 6) as a function of temperature for a 64 wt % 25R8 solution in D_2O.

The trend in Figure 15a is for the relative amplitudes of the fast and slow modes to vary such that the fast-mode amplitude increases and the slow-mode amplitude decreases with increasing concentration. Fits were also made using ILT analysis as exemplified in Figure 15b. The main peaks are invariably separated by two low-amplitude components. Here the discussion is restricted to the main decay features.

The relative amplitude of the fast mode is close to zero for c = 45 wt % at T = 60 °C and thereafter increases strongly with increasing concentration as shown in Figure 16. Furthermore, the shape of the distribution of the slow mode becomes narrower (i.e., β becomes larger) as the temperature is increased (Figure 17). Figure 18a shows data at three measurement angles for c = 64 wt % at 60 °C, and Figure 18b shows similar results of angular measurements at 90 °C on the same solutions. The fast and slow relaxation rates are plotted versus $\sin^2(\theta/2)$ for 60 °C in Figure 18c and for 90 °C in Figure 18d. At both temperatures, the fast relaxation rate is linearly dependent on the square of the scattering vector ($q \propto \sin(\theta/2)$)—i.e., it is a diffusive mode—while the slow mode is approximately independent of q and probably corresponds to structural relaxation of the viscous fluid.

Following the model used by Maechling-Strasser et al.[18] for hydrophobically end-capped poly(ethylene oxide) urethanes, the hydrophobic terminal PPO blocks are considered to associate locally into micelles which, in turn, are connected by the PEO chains. The interpretetation made here is that the delay time of the fast mode corresponds to the cooperative dynamics of the PEO segments and characterizes a mean correlation length (ξ) either in the large aggregates or in the gel.

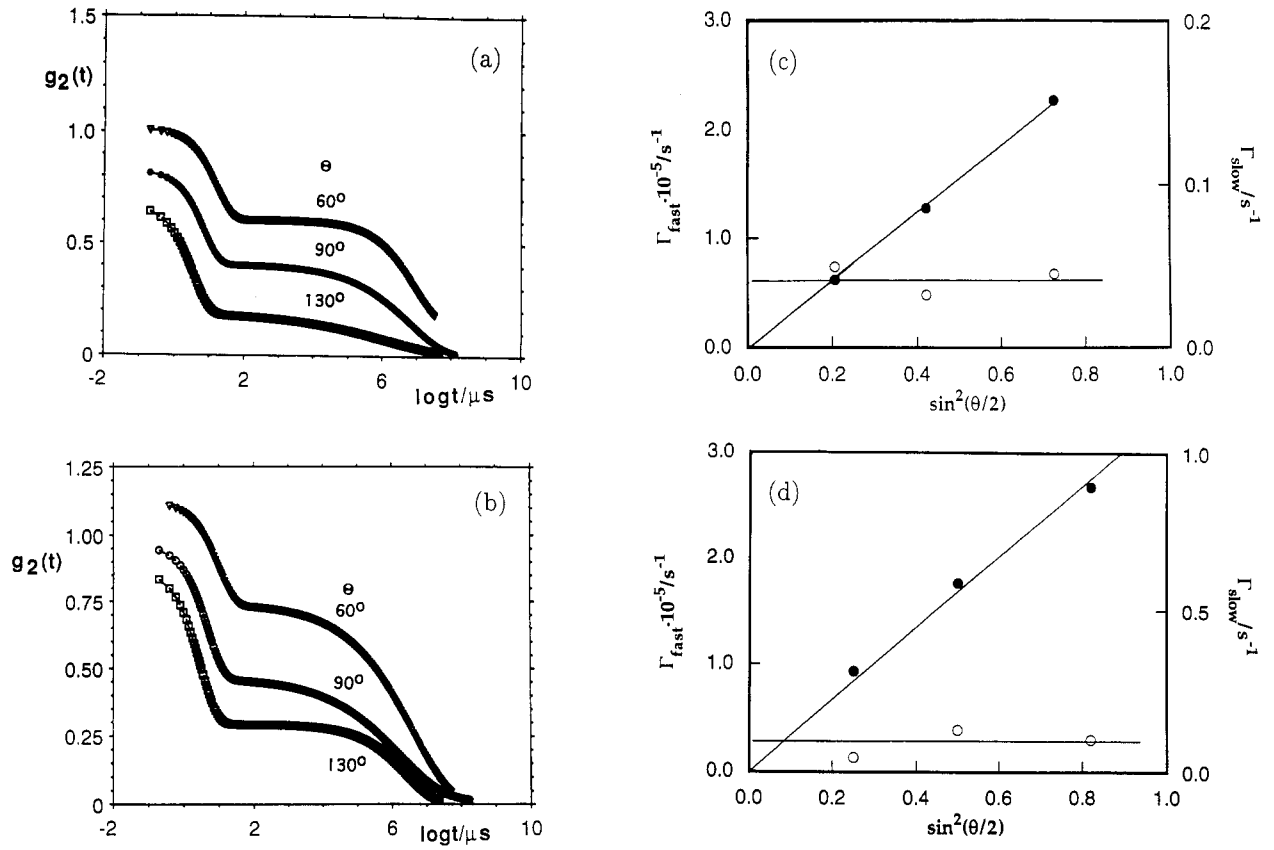

Figure 18. Correlograms at different angles for a 64 wt % solution of 25R8 in D_2O at (a) 60 and (b) 90 °C. Plots of relaxation rate (Γ) as a function of $\sin^2(\theta/2)$ for the fast and slow modes at (c) 60 and (d) 90 °C.

Correlation functions are shown in Figure 19a for the 73 wt % solution as a function of temperature. The corresponding activation energy is 5.2 kJ/mol ($\sim 2kT$) describing relaxation of the network nodes. It is seen that the relative amplitude of the relaxation mode decreases with increasing temperature (Figure 19b).

Figure 20a shows the ILT result for the fast end of the correlation functions given in Figure 15a. Figure 20b shows the correlation length (ξ) (derived using the Stokes–Einstein equation together with the solvent viscosity) as a function of concentration at 60 and 80 °C. The relaxation rate is essentially independent of concentration at both temperatures.

Figure 20c depicts the dynamic correlation length derived from the relaxation rate of the fast cooperative mode as a function of temperature for the data of 64 wt %.

That the correlation length is approximately independent of both copolymer concentration and temperature over the intervals studied implies that little interpenetration of the clusters occurs and that the correlation length reflects the PEO chain length whether the copolymer is present as an individual molecule or is in the gel phase. This is an essential difference compared to conventional gels (both permanent and transient) made up of long polymer chains which are characterized by a power law relation between the correlation length and the concentration owing to chain interpenetration. The average value of the correlation length in the present system is about 29 Å, which is similar to the hydrodynamic dimension of the individual copolymer molecule (23 Å). This strongly suggests that, on the addition of further copolymer, the hydrophobic end groups are simply accommodated into the gel structure with an approximately constant separation distance which is determined by the length of the PEO moiety.

DLS measurements were made on the c = 91 wt % solution at 90 °C. Even though multiple scattering reduces the intensity strongly, the correlation functions were approximately single exponential and the relaxation rate was q^2-dependent.

It is concluded that the suspension consists of large, randomly oriented, isotropic domains which are still able to diffuse slowly. This situation contrasts with that in the melt at high temperatures (see below), where the domains have a strongly anisotropic character.

D. Micellar Crystal. D1. Rheology. In the cooling scan of a 55 wt % sample (Figure 21), a first transition from liquid to a solid-like phase is seen at around 40 °C. These typical data for the elastic storage and loss shear moduli, G' and G'', are shown as a function of temperature. At temperatures above 40 °C $G'' > G'$, but G' shows a strong increase over a narrow interval of temperature and G' exceeds G'', marking a transition to a solid-like phase. These observations resemble the rheological data observed in aqueous solutions of PEO–PPO–PEO micelles when crossing the transition from micellar liquid to the cubic phase of ordered micelles.[2]

This transition is observed for all samples above 45 wt % (Figure 22); however, some preparation dependence appears for suspensions with polymer concentration below 50 wt %. Only 1–2 °C in hysteresis is seen in the transition temperature by following heating scans.

The trend from Figure 11 with higher viscosity at 55–60 wt % samples is followed here by the hardest solid-like structure at these concentrations and softer structures at both higher and lower concentrations.

A strain dependence is observed in the solid-like phase, as shown in Figure 23. For strain amplitudes above 0.01 the elastic moduli decrease markedly with strain.

D2. Neutron Scattering. While most 25R8 suspensions show azimuthally isotropic scattering patterns, the

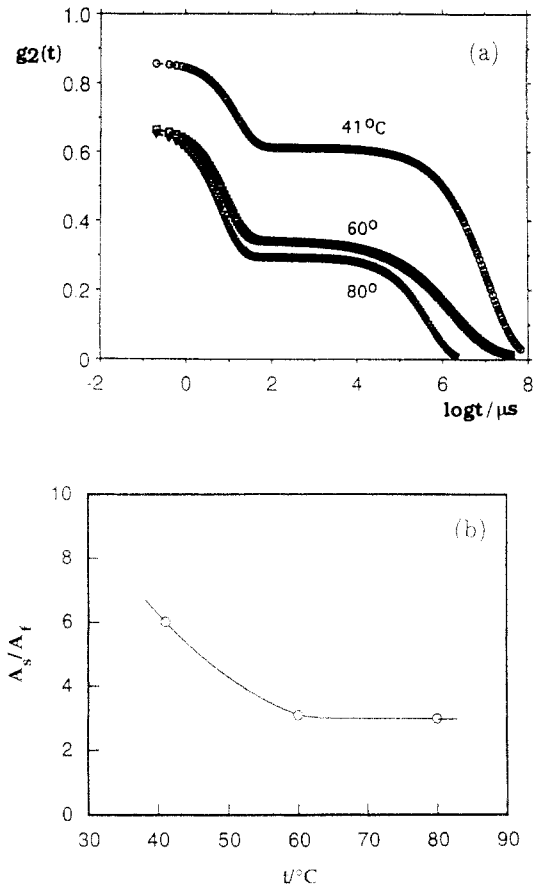

Figure 19. (a) Dynamic light scattering correlograms for a 73 wt % solution of 25R8 in D_2O at (from top to bottom) T = 41, 60, and 80 °C. Measurements at 90° in the VV geometry. (b) Ratio of amplitude of slow to fast modes as a function of temperature for c = 73 wt %.

65 wt % sample shows marked texture when measured at temperatures below T_c = 40 °C, as shown in Figure 24. Simultaneously, the line width of the correlation peak exhibits a small, but significant change (Figure 5). This behavior indicates long-range order in the micellar organization for $T < T_c$.

The change in line width reflects a sudden change in the micellar volume fraction from ϕ = 0.48 for $T \geq T_c$ = 40 °C to ϕ = 0.53 for temperatures T < 40 °C. The volume fraction ϕ = 0.53 is the critical value for hard-sphere crystallization into a cubic lattice, as observed for PEO–PPO–PEO micellar solutions[3] as well as in classical colloidal systems.[23] We therefore conclude that 25R8 also forms a cubic mesophase.

E. Elastic Lamellar Gel. At high concentrations and low temperatures, 25R8 forms a two-phase system with elastic properties.

E1. Rheology. Rheological measurements show (Figures 21 and 22) that below approximately 30 °C a second transition occurs. These transitions from a softer solid-like phase to a harder solid-like phase do not show the same reproducibility as the first transition in either the elastic moduli values or the transition temperatures. Hysteresis is clearly seen for this transition and can in a heating scan disturb the high-temperature transition, with hysteresis as a result for this one as well. These observations are in good agreement with the conclusion from light and neutron scattering that the material in this part of the phase diagram is decomposed into two separate phases, as discussed below. In the light and neutron scattering experiments the two-phase range is, though, observed only at somewhat lower temperatures and higher copolymer concentrations.

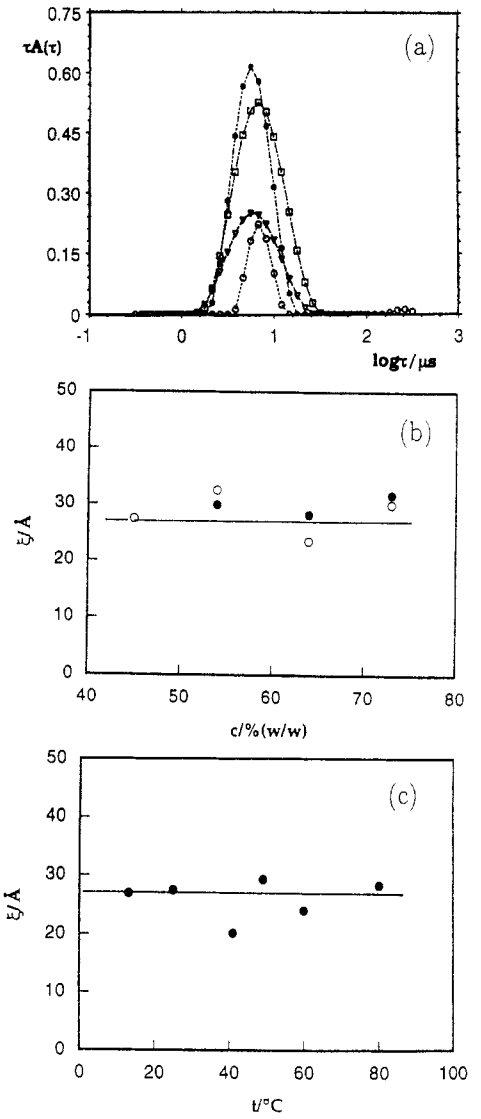

Figure 20. (a) Inverse Laplace transform results for the fast mode at the concentrations 73 (●), 64 (□), 54 (△), and 45 wt % (○) at 80 °C. (b) Plot of the dynamic correlation length ξ versus concentration (from the collective diffusion coefficient using the Stokes–Einstein equation) for DLS data at 80 (●) and 60 °C (○). (c) Temperature dependence of dynamic correlation length for c = 64 wt %.

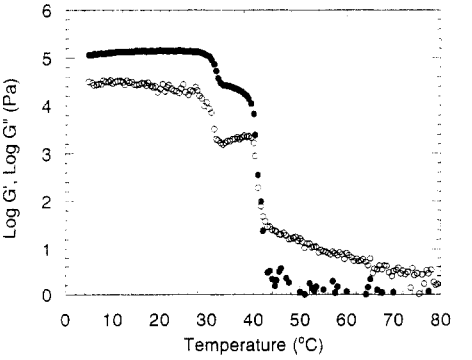

Figure 21. Storage and loss moduli, G' (●) and G'' (○), from oscillatory shear measurements on a 55 wt % 25R8 suspension measured at a frequency of 0.15 Hz as a function of temperature.

The 45 wt % sample is the lowest concentration which shows solid-like phases, and for the low-temperature solid-like phase, the 45 wt % sample shows the lowest elastic moduli. The elastic moduli increase with concentration up till 55 wt %. Above this concentration the moduli seem to reach a constant level just above 100 kPa.

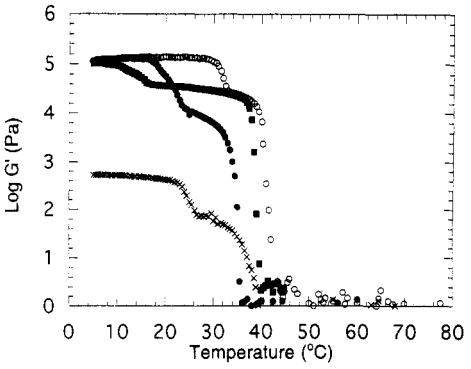

Figure 22. Storage modulus, G', of 25R8 suspensions at the concentrations 45 (×), 55 (○), 60 (□) and, 75 wt % (●) versus temperature measured by oscillatory shear studies at a frequency of 0.15 Hz.

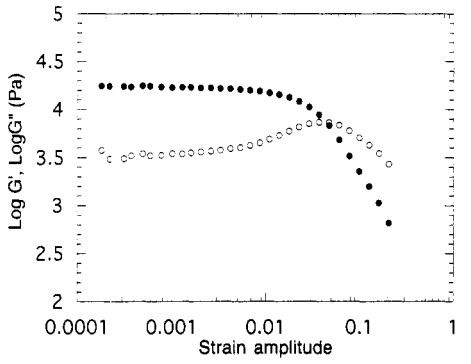

Figure 23. Storage and loss moduli, G' (●) and G'' (○), from oscillatory shear measurements on a 55 wt % 25R8 suspension measured at a frequency of 0.15 Hz as a function of temperature.

This solid-like phase shows a strain dependence similar to the first solid-like phase. Thus here there is a weak dependence between strain amplitudes of 0.0001 and 0.005 where G' decreases with strain, but a dramatic dependence is seen at strain amplitudes above 0.005 where G' drops markedly.

E2. Neutron Scattering. The neutron scattering pattern of the high-concentration gel shows characteristics of highly anisotropic aggregates. The scattering intensity is characterized by a rather intense zero-q scattering and a side maximum at $q = 0.03$ Å^{-1}. In addition, the scattering pattern shows over the whole temperature range a peak at $q \sim 0.05$ Å^{-1}. The temperature dependences of these three characteristics—zero-q intensity and the two peaks—follow different trends, indicating multiphase behavior at low temperatures.

Upon exposure to external shear, the scattering pattern shows marked anisotropic character, as seen in the contour plots of Figure 25. The small-angle scattering shows basically ellipsoidal character, with the short axis parallel to the flow, indicating scattering from anisotropic aggregates of rod-like or pancake-like form. Both the $q \sim 0.03$ Å^{-1} peak and the $q \sim 0.05$ Å^{-1} peak are located in orientations perpendicular to the flow.

When heated above approximately $T = 35$ °C, both the anisotropic character and the $q \sim 0.03$ Å^{-1} peak vanish, and a single phase appears dominated by the $q \sim 0.05$ Å^{-1} correlation peak.

The pure 25R8 melt forms a lamellar mesophase at low temperatures, as shown below. With this information in mind, we interpret the low-q scattering of the 80% sample as a two-phase system given by (i) swollen lamellae and (ii) micelles. Equivalent two-phase systems have been observed in high-concentration PEO–PPO–PEO types of suspensions.[24] The lamellar correlation peak at $q \sim 0.03$

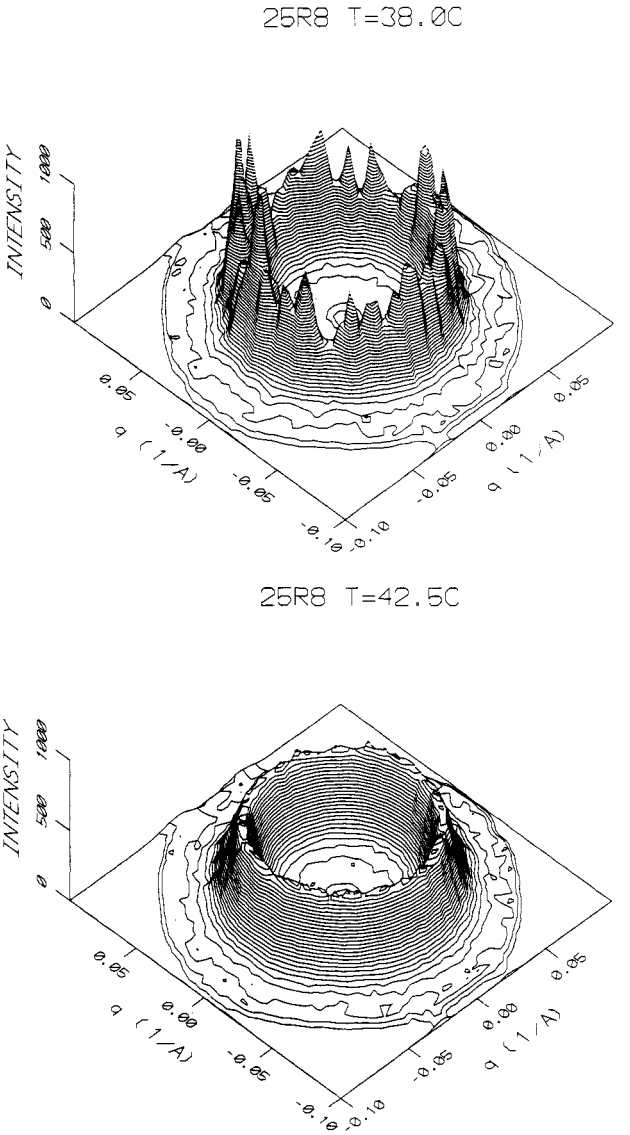

Figure 24. Surface plots of the neutron scattering pattern obtained from 65 wt % 25R8 as measured at $T = 38.0$ °C and $T = 42.5$ °C.

Å^{-1} signifies that the lamellar domains of the 80% 25R8 suspension are swollen approximately 20% relative to the pure 25R8 melt.

Upon increasing temperature, the lamellar domains vanish at the expense of the micellar network, which constitutes the whole sample above $T = 35$ °C.

F. 25R8 Triblock Copolymer Melt. F1. Neutron Scattering. Figure 26 shows the scattering pattern of the 25R8 melt as observed at room temperature. The scattering function clearly reveals a lamellar structure, with both first- and second-order peaks. The lamellar periodicity is $d = 2\pi/q_0 = 175$ Å, where $q_0 = 0.036$ Å^{-1} is the scattering momentum of the first-order peak. The marked small-angle scattering reveals that the sample is not homogeneous but includes a number of vacancies, which can also be observed looking at the sample. The lamellar spacing is large relative to the unimer radius of gyration $R_g = 37$ Å, indicating highly stretched polymers, possibly a result of the crystalline PEO domains.

The lamellar structure remains basically unaffected up to the melting temperature at $T_m = 55$ °C. Above this temperature, there is, within experimental resolution, no correlation peak at all (Figure 27). This is quite different from observations on amorphous block copolymers, where typically there is only a relatively small change in peak

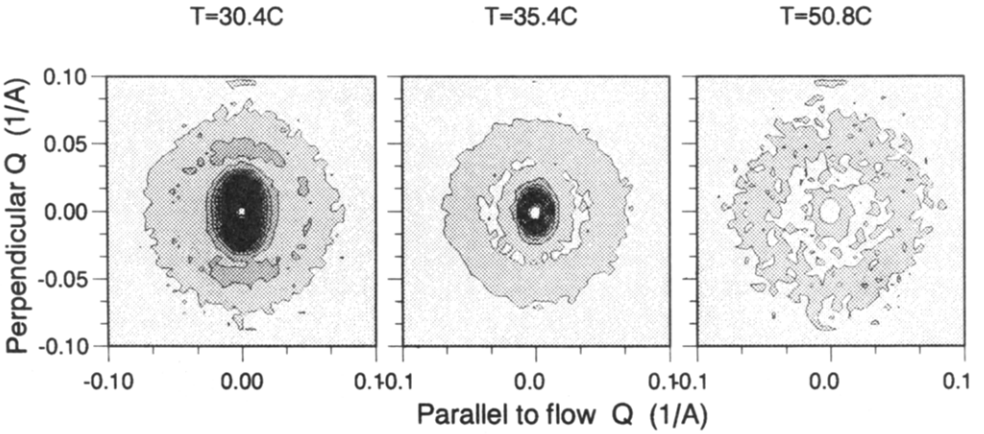

Figure 25. Contour plots of the neutron scattering pattern obtained from 80 wt % 25R8 as measured at T = 30.4 °C, T = 35.4 °C, and T = 50.8 °C. The measurements were performed while the suspension was exposed to a 100 s^{-1} shear rate. The flow direction is horizontal in the figure, and the shear gradient was parallel to the neutron beam (perpendicular to the contour planes).

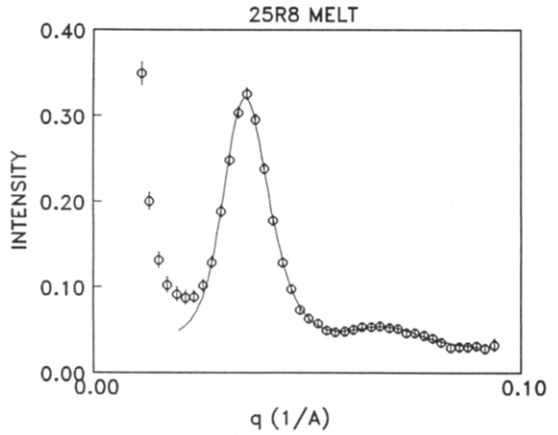

Figure 26. Neutron scattering of the 25R8 melt, T = 25 °C. The solid line is fit to two Lorentzian lines centered at q_0 and q_1. Within statistics, $q_1 = 2q_0$, showing the lamellar structure.

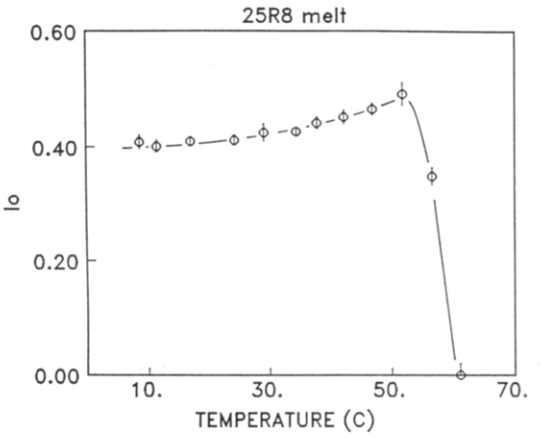

Figure 27. Peak intensity of first-order reflection from the lamellar structure of 25R8 as a function of temperature.

intensity on crossing the order–disorder transition (ODT). Above the ODT, a pronounced Leibler peak appears due to spatial concentration fluctuations.[25]

The peak intensity is, however, not only given by the amplitude of the concentration fluctuations but also by the scattering contrast between the two types of polymer blocks. In the 25R8 block copolymer melt, there is significant contrast between PEO and PPO only because the PEO block is crystalline whereas PPO is amorphous, thus resulting in a marked mass-density difference. For T_m > 55 °C PEO is amorphous, too, and the scattering contrast vanishes. It is therefore not possible to follow composition fluctuations above the PEO melting temperature. Future studies should include partly deuterated copolymers in which sufficient contrast can also be obtained in the amorphous regime.

F2. Light Scattering. Dynamic light scattering measurements were made on the melt copolymer. Since the melt was found to exhibit substantial optical anisotropy, measurements were made on the glass-clear fluid at 90 °C in the depolarized (VH) geometry. Correlation functions at three angles are shown in Figure 28a. The correlation functions are, perhaps unexpectedly, q^2-dependent as shown in Figure 28b and the intensity is also q-dependent (Figure 28c). A similar phenomenon was recently demonstrated by Fytas et al.[26] for an asymmetric diblock copolymer in solution at temperatures close to the order–disorder transition (ODT). The interpretation was made there that a large form anisotropy exists in the ordered state owing to the microstructure of the domains. By analogy, the anisotropic domains present in 25R8 melts also exhibit translational/rotational coupling. A similar observation was made for the melt of the triblock copolymer PEO–PPO–PEO (P85) recently examined.[24]

IV. Conclusion

In conclusion, we have shown that the PPO–PEO–PPO triblock copolymers have complex phase behavior when dissolved in water (D_2O), depending on both copolymer concentration and temperature. Figure 29 shows the resulting phase diagram of 25R8.

At low temperatures and high dilution the copolymer exists in solution as individual molecules, unimers. The scattering pattern reveals a Gaussian conformation.

Upon increasing the temperature or polymer concentration, association of poly(propylene oxide) moieties leads to various networks, as illustrated in Figure 30. Association of the PPO units is driven by the tendency to minimize PPO–water contacts. Thus, while at high dilution the copolymer can exist in solution as individual molecules, intermolecular association of the PPO moieties increases as the concentration is increased.

For relatively low concentrations (c < 0.4) of the copolymer suspension, the hydrophobic nature of PPO at elevated temperatures leads to association, which may occur in a wide variety of ways as has been illustrated in ref 18. It will eventually lead to a very inhomogeneous polydisperse suspension of randomly cross-linked networks as illustrated in Figure 30. Such network clusters may differ greatly in size. PPO association may be formed by both intra- and intermolecular contacts. The network is

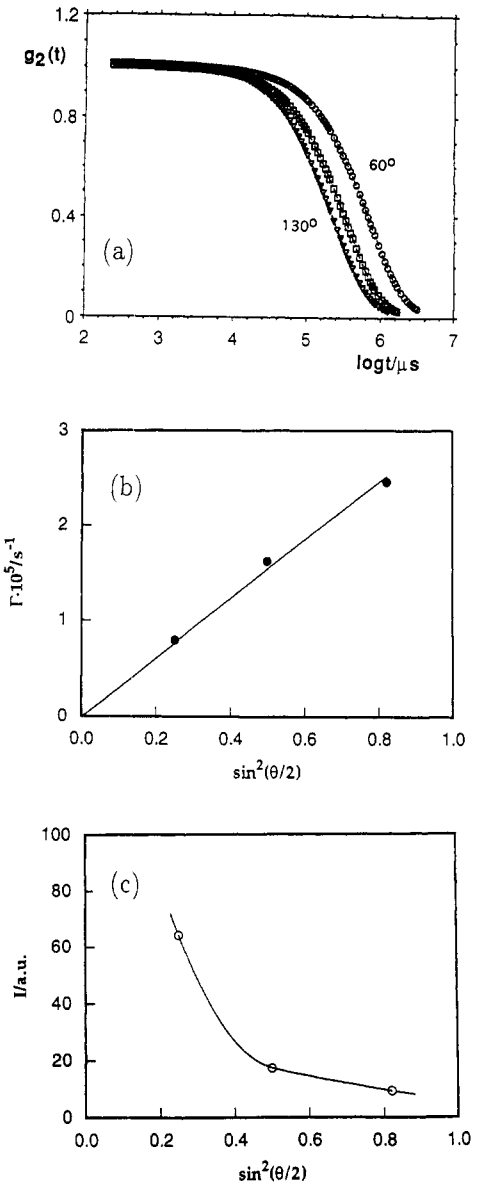

Figure 28. Depolarization (VH geometry) dynamic light scattering correlograms for the 25R8 melt at 90 °C (angles from right to left: 60, 90, and 130°). (b) Relaxation rate as a function of $\sin^2(q/2)$. (c) Angle dependence of the depolarized scattering intensity for the 25R8 melt at 90 °C.

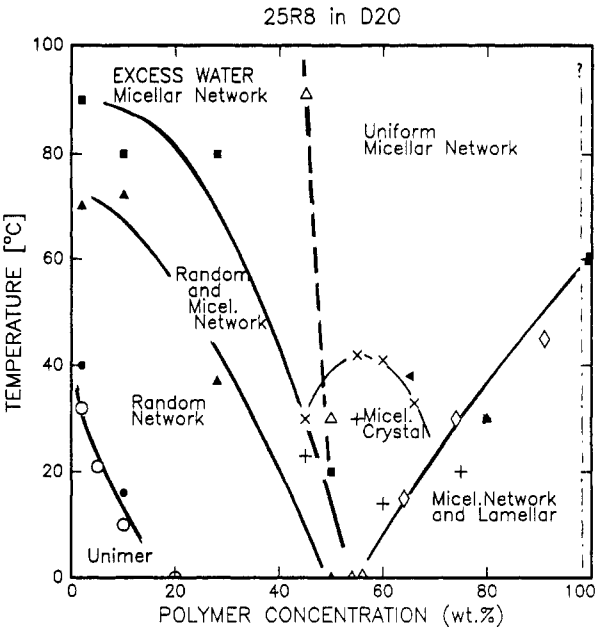

Figure 29. Phase diagram of the Pluronic-R system 25R8. Closed symbols refer to neutron scattering results, open symbols to light scattering, and crosses to rheological data (see text).

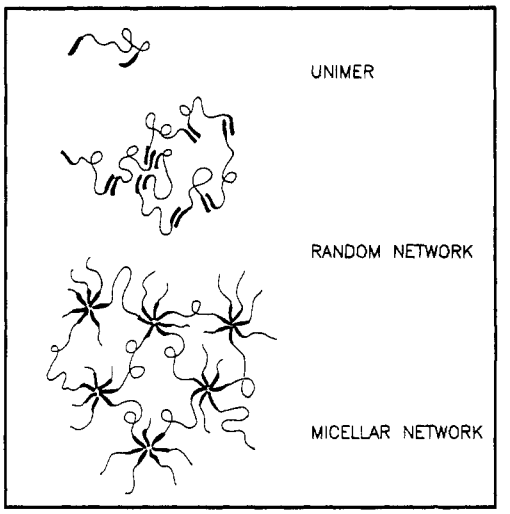

Figure 30. Schematic describing the different phases: random coil, random network, and micellar network.

temporary in the sense that junctions which hold the network together can break and re-form on a short time scale.

At higher temperatures or higher copolymer concentrations, the PPO associates into a core of rather well-defined spherical micelles. These micelles are interconnected by the hydrophilic PEO blocks, resulting in a micellar network, as illustrated in Figure 30. Suspensions of the micellar network therefore show liquid-like, Newtonian viscosity at the frequency of measurement.

Only in a rather small part of the phase diagram, namely, at low temperatures and copolymer concentrations between 50 and 70 wt %, is a micellar mesophase formed as a result of hard-sphere crystallization. In this phase the micellar aggregates are arranged on a regular geometric lattice, presumably cubic. The micellar suspension forms in this phase a solid-like elastic gel.

At the highest copolymer concentrations and low temperatures, the suspensions form a two-phase system with elastic properties. It are proposed that the elasticity results from the dominating lamellar domain structure. The phase separation kinetics are slow, resulting in only qualitative reproducibility in neutron scattering data (i.e., the relative influence in the scattering pattern of the two domains depends on history). This is further evident looking at the samples: when the concentrated solution (for example, that of c = 73 wt %) is cooled to about ambient temperature, an array of small opaque spheres is formed which are interspersed by clear material. On standing for some hours, the small aggregates grow in size. The c = 64 wt % solution displays similar behavior but incipient phase separation only occurs visually at a lower temperature of about 6 °C.

Below $T_m \sim 55$ °C, the PEO and PPO blocks of the 25R8 melt micro-phase separate and form a lamellar mesophase. The PEO block is crystalline in this phase. The ODT is not known but may coincide with the melting of PEO. Above T_m, however, optical anisotropy is observed, reflecting significant structure in the molecular arrangement.

Acknowledgment. The authors acknowledge financial support from the Danish and the Swedish Natural Science Research Councils.

References and Notes

(1) Wanka, G.; Hoffmann, H.; Ulbricht, W. *Colloid Polym. Sci.* **1990**, *268*, 101–117.
(2) Brown, W.; Schillén, K.; Almgren, M.; Hvidt, S.; Bahadur, P. *J. Phys. Chem.* **1991**, *95*, 1850–1858.
(3) Mortensen, K.; Brown, W.; Nordén, B. *Phys. Rev. Lett.* **1992**, *68*, 2340–2343.
(4) Mortensen, K. *Europhys. Lett.* **1992**, *19*, 599–604.
(5) Wu, G.; Zhou, Z.; Chu, B. *Macromolecules* **1993**, *26*, 2117–2125.
(6) Yu, G.-E.; Deng, Y.; Dalton, S.; Wang, Q.-G.; Attwood, D.; Booth, C. *J. Chem. Soc., Faraday Trans.* **1992**, *88*, 2537–2544.
(7) Mortensen, K.; Pedersen, J. S. *Macromolecules* **1993**, *26*, 805–812.
(8) Wanka, G.; Hoffmann, H.; Ulbricht, W. *Macromolecules*, submitted.
(9) Linse, P.; Malmsten, M. *Macromolecules* **1992**, *25*, 5434–5439.
(10) Fleischer, G. *J. Phys. Chem.* **1993**, *97*, 517–521.
(11) Mortensen, K.; Brown, W. *Macromolecules* **1993**, *26*, 4128–4135.
(12) BASF Report *Pluronic and Tetronic Surfactants*, BASF Wyandotte, 1989.
(13) Nordén, B.; Elvingson, C.; Eriksson, T.; Kubista, M.; Sjöberg, B.; Takahashi, M.; Mortensen, K. *J. Mol. Biol.* **1990**, *216*, 223.
(14) Pedersen, J. S.; Posselt, D.; Mortensen, K. *J. Appl. Crystallogr.* **1990**, *23*, 321.
(15) Nicolai, T.; Brown, W.; Johnsen, R. M.; Štěpánek, P. *Macromolecules* **1990**, *23*, 1165.
(16) Mischenko, N.; Reynders, K.; Mortensen, K.; Scherrenberg, R.; Fontaine, F.; Graulus, R.; Reynaers, H. *Macromolecules* **1994**, *27*, 2345.
(17) Alami, E.; Rawiso, M.; Isel, F.; Beinert, G.; Limbele, W. B.; Francois, J., preprint.
(18) Maechling-Strasser, C.; Clouet, F.; Francois, J. *Polymer* **1992**, *33*, 1021.
(19) Baxter, R. J. *J. Chem. Phys.* **1968**, *49*, 2770.
(20) Guinier, A.; Fournet, G. *Small Angle Scattering of X-Rays*; Wiley: New York, 1955.
(21) Percus, J. K.; Yevick, G. J. *Phys. Rev.* **1958**, *110*, 1.
(22) Menon, S. V. G.; Monohar, C.; Rao, K. S. *J. Chem. Phys.* **1991**, *95*, 9186.
(23) Pusey, P. N.; van Megen, W. *Nature (London)* **1986**, *320*, 340.
(24) Mortensen, K.; Brown, W. *Macromolecules*, submitted.
(25) Almdal, K.; Bates, F. S.; Mortensen, K. *J. Chem. Phys.* **1992**, *96*, 9122.
(26) Jian, T.; Anastasiadis, H.; Fytas, G.; Adachi, K.; Kotaka, T. *Macromolecules* **1993**, *26*, 4706.